

Article

Transition from ferromagnetic semiconductor to ferromagnetic metal with enhanced Curie temperature in CrGeTe via organic ion intercalation

Naizhou Wang, Huaibao Tang, Mengzhu Shi, Hui Zhang, Weizhuang Zhuo, Dayong Liu, Fanbao Meng, Likuan Ma, Jianjun Ying, Liangjian Zou, Zhe Sun, and Xianhui Chen

J. Am. Chem. Soc., Just Accepted Manuscript • DOI: 10.1021/jacs.9b06929 • Publication Date (Web): 10 Oct 2019

Downloaded from pubs.acs.org on October 12, 2019

Just Accepted

"Just Accepted" manuscripts have been peer-reviewed and accepted for publication. They are posted online prior to technical editing, formatting for publication and author proofing. The American Chemical Society provides "Just Accepted" as a service to the research community to expedite the dissemination of scientific material as soon as possible after acceptance. "Just Accepted" manuscripts appear in full in PDF format accompanied by an HTML abstract. "Just Accepted" manuscripts have been fully peer reviewed, but should not be considered the official version of record. They are citable by the Digital Object Identifier (DOI®). "Just Accepted" is an optional service offered to authors. Therefore, the "Just Accepted" Web site may not include all articles that will be published in the journal. After a manuscript is technically edited and formatted, it will be removed from the "Just Accepted" Web site and published as an ASAP article. Note that technical editing may introduce minor changes to the manuscript text and/or graphics which could affect content, and all legal disclaimers and ethical guidelines that apply to the journal pertain. ACS cannot be held responsible for errors or consequences arising from the use of information contained in these "Just Accepted" manuscripts.

Transition from ferromagnetic semiconductor to ferromagnetic metal with enhanced Curie temperature in $\text{Cr}_2\text{Ge}_2\text{Te}_6$ via organic ion intercalation

Naizhou Wang,^{1,†} Huaibao Tang,^{2,†} Mengzhu Shi,¹ Hui Zhang,² Weizhuang Zhuo,¹ Dayong Liu,³ Fanbao Meng,¹ Likuan Ma,¹ Jianjun Ying,¹ Liangjian Zou,^{3,*} Zhe Sun,⁴ Xianhui Chen^{1,5,6,7*}

¹Hefei National Laboratory for Physical Sciences at Microscale and Department of Physics, and Key Laboratory of Strongly-coupled Quantum Matter Physics, University of Science and Technology of China, Hefei 230026, Anhui, China

²School of Physics and Materials Science, Anhui University, Hefei 230039, Anhui, China

³Key Laboratory of Materials Physics, Institute of Solid State Physics, Chinese Academy of Sciences, Hefei 230031, Anhui, China

⁴National Synchrotron Radiation Laboratory, University of Science and Technology of China, Hefei, Anhui 230026, China

⁵Collaborative Innovation Center of Advanced Microstructures, Nanjing University, Nanjing 210093, China

⁶CAS Center for Excellence in Superconducting ionics (CENSE), Shanghai 200050, China

⁷CAS Center for Excellence in Quantum Information and Quantum Physics, Hefei, Anhui 230026, China

ABSTRACT: Magnetism in two-dimensional limit has become an intriguing topic for exploring new physical phenomena and potential applications. Especially, the two-dimensional magnetism is often associated with novel intrinsic spin fluctuations and versatile electronic structures, which provides vast opportunities in 2D material research. However, it is still challenging to verify candidate materials hosting two-dimensional magnetism, since the prototype systems have to be realized by using mechanical exfoliation or atomic layer deposition. Here, an alternative manipulation of two-dimensional magnetic properties via electrochemical intercalation of organic molecules is reported. Using tetrabutyl ammonium (TBA^+), we synthesized $(\text{TBA})\text{Cr}_2\text{Ge}_2\text{Te}_6$ hybrid superlattice with metallic behavior, and the Curie temperature is significantly increased from 67 K in pristine $\text{Cr}_2\text{Ge}_2\text{Te}_6$ to 208 K in $(\text{TBA})\text{Cr}_2\text{Ge}_2\text{Te}_6$. Moreover, the magnetic easy axis changes from the $\langle 001 \rangle$ direction in $\text{Cr}_2\text{Ge}_2\text{Te}_6$ to the ab-plane in $(\text{TBA})\text{Cr}_2\text{Ge}_2\text{Te}_6$. Theoretical calculations indicate that the drastic increase of Curie temperature can be attributed to the change of magnetic coupling from weak super-exchange interaction in pristine $\text{Cr}_2\text{Ge}_2\text{Te}_6$ to strong double exchange interaction in the $(\text{TBA})\text{Cr}_2\text{Ge}_2\text{Te}_6$. These findings are the first demonstration of manipulation of magnetism in magnetic van der Waals materials by means of intercalating organic ions, which can serve as a convenient and efficient approach to explore versatile magnetic and electronic properties in van der Waals crystals.

INTRODUCTION

Accumulating interest in two-dimensional materials has triggered great attention in the studies of atomically thin van der Waals crystals, owing to their novel physical properties and versatile electronic structures.^{1,2,3} In particular, 2D magnetism in these materials opens up vast possibilities for both fundamental research and future application.⁴ Moreover, the desirable controllability of

structures and chemical compositions makes it possible to induce various magnetic orders and enhance spin fluctuations.⁴ The development of this field has been boosted recently by the discovery of intrinsic ferromagnetic order in few layers and monolayer van der Waals crystals, such as $\text{Cr}_2\text{Ge}_2\text{Te}_6$, CrI_3 and Fe_3GeTe_2 .^{5,6,7}

In magnetic van der Waals materials, the Curie temperature shows a strong dimensional dependence.

The persistence of the long-range ferromagnetic order in 2D limit is due to the intrinsic magnetocrystalline anisotropy, accompanied by the opening up of a non-zero excitation gap in the low energy mode of the acoustic magnon branch.⁵ At a finite temperature T_c , the thermal energy would excite a large number of low-energy magnon modes to destroy the long-range magnetic order. With increasing the layer numbers, the density of states near the excitation gap decreases, which indicates that a higher T_c is needed to assure a sufficient number of excitations to break the long-range magnetic order.⁵ Therefore, the critical T_c shows evident dimensional dependence.

Field effect transistor (FET) configurations are usually employed to tune carrier concentration and consequently manipulate the magnetism in 2D magnetic van der Waals crystals,⁷⁻¹¹ in which the magnetic properties including saturation magnetization, coercive force and Curie temperature vary strongly as the function of charge doping.⁸⁻¹⁰ Nevertheless, the difficulties in fabrication and characterization of FET devices have limited further explorations of novel magnetic and electronic properties in candidate materials. Therefore, it is crucial to find a convenient and efficient way to tune the electronic states and magnetism in van der Waals materials. The electrochemical organic ion intercalation is an alternative route, since the organic ion intercalation could not only tune the carrier concentration but also reduce the interlayer coupling and change the dimensionality of the system.¹²⁻¹⁴

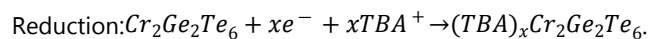
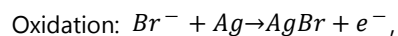
Here we report the drastic enhancement of ferromagnetic transition temperature in $\text{Cr}_2\text{Ge}_2\text{Te}_6$ via electrochemical intercalation of tetrabutyl ammonium (TBA^+). In our studies, the single crystal $\text{Cr}_2\text{Ge}_2\text{Te}_6$ is intercalated with TBA^+ cations to form a hybrid superlattice $(\text{TBA})\text{Cr}_2\text{Ge}_2\text{Te}_6$. Surprisingly, the $(\text{TBA})\text{Cr}_2\text{Ge}_2\text{Te}_6$ shows metallic behavior and the Curie temperature is significantly increased from 67 K in pristine $\text{Cr}_2\text{Ge}_2\text{Te}_6$ semiconductor to 208 K. Moreover, the magnetic easy axis of $(\text{TBA})\text{Cr}_2\text{Ge}_2\text{Te}_6$ is reoriented to the ab plane from the c-axis in pristine $\text{Cr}_2\text{Ge}_2\text{Te}_6$. Theoretical calculations indicate that the $\text{Cr}_2\text{Ge}_2\text{Te}_6$ layers are electron doped and the ground state of $\text{Cr}_2\text{Ge}_2\text{Te}_6$ is altered from semiconductor to metal. Consequently, the ferromagnetism arises from the coupling between conduction electrons and local spins in $(\text{TBA})\text{Cr}_2\text{Ge}_2\text{Te}_6$, instead of the weak super-exchange interaction in $\text{Cr}_2\text{Ge}_2\text{Te}_6$, which results in a large increase of Curie temperature.

EXPERIMENTAL SECTION

Synthesis of $\text{Cr}_2\text{Ge}_2\text{Te}_6$ single crystal. The high-quality single crystals of $\text{Cr}_2\text{Ge}_2\text{Te}_6$ were synthesized using the

flux method.¹⁵ Cr powder (Aladdin, 99.5%), Ge powder (Alfa Aesar, 99.999%) and Te powder (Alfa Aesar, 99.999%) were mixed and grounded with a mole ratio of 2:6:36 in argon atmosphere. The mixture was then sealed in a silica ampoule under high vacuum. The sealed ampoule was heated to 700 °C and held for 20 days, and then slowly cooled to 500 °C in 1.5 days, followed by centrifugation treatment to remove Te flux. In order to get rid of the residual Te flux on the surface of $\text{Cr}_2\text{Ge}_2\text{Te}_6$ crystals, the samples were annealed at 400 °C in a horizon, two-zone furnace with a temperature gradient. The typical size of $\text{Cr}_2\text{Ge}_2\text{Te}_6$ single crystals is 3 mm x 3 mm x 0.03 mm.

Electrochemical intercalation of $\text{Cr}_2\text{Ge}_2\text{Te}_6$ with TBA^+ . Before the electrochemical intercalation, the single crystals of $\text{Cr}_2\text{Ge}_2\text{Te}_6$ were washed with ethanol and cut into regular pieces. The mass of each single crystal was accurately weighted with a high precision balance. Then, single crystals were pressed onto an indium plate and acted as the positive electrode. A 0.2 mm thick silver piece was used as the negative electrode. A supersaturated solution of TBAB (Tetrabutyl ammonium bromide) powder (Aladdin, 99.0%) dissolved in DMF (Innochem, 99.9%, extra dry with molecular sieves, water less than 50 ppm) was used for the intercalation process. In order to realize a uniform intercalation, a constant current of 2 μA was applied to control the electrochemical intercalation. The whole intercalation process was controlled by Lanhe testing system and carried out in an argon-filled glove box. During the intercalation process, the negative electrode loses electrons, while the positive electrode obtains electrons. The process is described by the following equations:



The amount of intercalated TBA^+ , namely x in $(\text{TBA})_x\text{Cr}_2\text{Ge}_2\text{Te}_6$, is determined by the current passing through the cell and the electro-duration of galvanostatic discharge process. The galvanostatic discharge curve of $(\text{TBA})_x\text{Cr}_2\text{Ge}_2\text{Te}_6$ is shown in supporting information S1. The similar method is also used to determine the intercalation amount of Li in Li_xMoS_2 and Li_xNbSe_2 .^{16,17} The amount of intercalated TBA^+ , namely x in $(\text{TBA})_x\text{Cr}_2\text{Ge}_2\text{Te}_6$, is calculated according to following formula:

$$t = \frac{Fmx}{MI}$$

t is the time of galvanostatic discharge process, F is the Farady constant (96485.31 C mol⁻¹), m is the mass of pristine $\text{Cr}_2\text{Ge}_2\text{Te}_6$ single crystal, x is the amount of intercalated TBA^+ , M is the molar mass of $\text{Cr}_2\text{Ge}_2\text{Te}_6$, I is the electric current passing through the cell. In the

intercalation process, the x in $(TBA)_xCr_2Ge_2Te_6$ was set to be 1.0 to achieve a uniform and single-phase intercalation. When $x < 1.0$, un-intercalated $Cr_2Ge_2Te_6$ phase remains in X-ray diffraction patterns. When $x > 1.0$, the morphology of single crystal would be destroyed.

Characterizations of the $(TBA)Cr_2Ge_2Te_6$. The X-ray diffraction patterns of pristine and intercalated sample were collected on a diffractometer (Rigaku SmartLab 9KW) equipped with $Cu K\alpha$ radiation and a fixed graphite monochromatic. The high-resolution transmission electron microscopy (HRTEM) images of $Cr_2Ge_2Te_6$ and intercalated $(TBA)Cr_2Ge_2Te_6$ were acquired by a Talos F200X microscope at 200 kV and a Jeol 2010 microscope at 200 kV, respectively. The magnetic susceptibility measurement was carried out using a SQUID magnetometer (Quantum Design MPMS-5). The resistivity measurement was conducted on a physical property measurement system (Quantum Design PPMS-9T) with the standard four-terminal method. In order to prevent damage from oxygen and moisture, the preparation for transport measurements was conducted in a glove box, and the samples were sealed in a chip carrier (ceramic dual-in-line chip carriers) with vacuum grease and covered a piece of glass. Once ready, the whole package is immediately inserted into the PPMS.

Theoretical calculation. First-principles calculations based on density functional theory (DFT) were performed using the full-potential augmented plane wave plus local orbital code (Wien2k). ¹⁸The exchange-correlation interaction was treated with the generalized gradient approximation (GGA) parameterized by Perdew-Burke-Ernzerhof formula.¹⁹ To improve the description of on-site Coulomb interaction between Cr 3d electrons, we adopted the GGA+U scheme with the typical values of the Hubbard U = 0.5 eV for the bulk $Cr_2Ge_2Te_6$ and 0.2 eV for $(TBA)Cr_2Ge_2Te_6$.⁵ Furthermore, the relativistic spin-orbit coupling (SOC) is included by the second-variational method with scalar relativistic wave functions to determine the magnetic anisotropy energy (MAE). The sphere radii of 2.38, 2.50 and 2.27 Bohr were chosen for Te, Cr and Ge atoms, respectively. The basis set cut-off parameter $R_{mt}K_{max} = 7.0$ was found to be sufficient. For the Brillouin zone integrations, k-point meshes of $12 \times 12 \times 4$ and $10 \times 10 \times 2$ were used for pristine and intercalated $Cr_2Ge_2Te_6$, respectively.

RESULTS AND DISCUSSION

High-quality $Cr_2Ge_2Te_6$ single crystals were used as the host material to conduct the electrochemical intercalation.

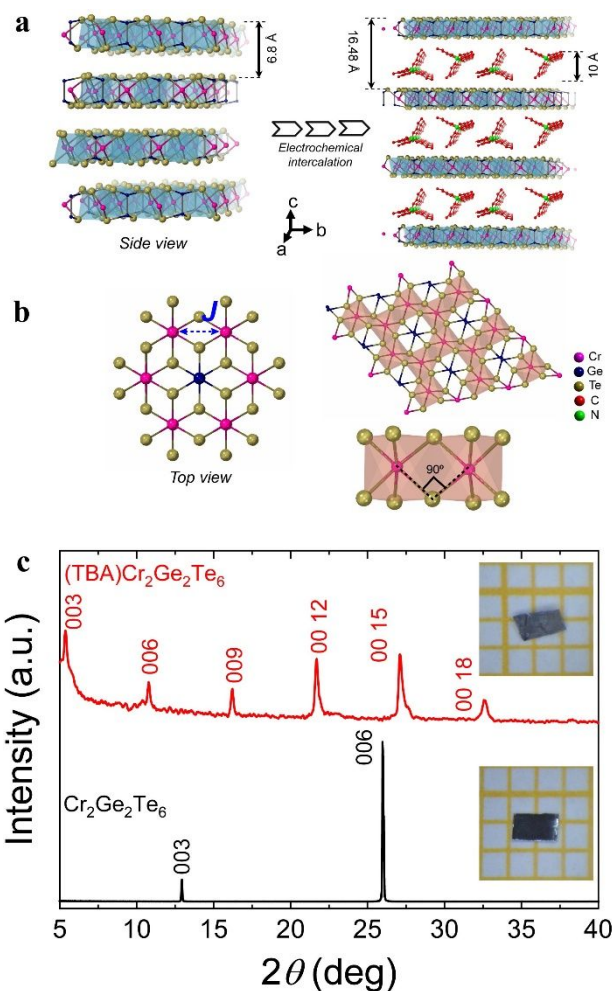


Figure 1. The schematic structure model of $(TBA)Cr_2Ge_2Te_6$. (a): The side-view crystal structure of $Cr_2Ge_2Te_6$ and $(TBA)Cr_2Ge_2Te_6$. The space group of pristine $Cr_2Ge_2Te_6$ is R-3 (No. 148). Pristine $Cr_2Ge_2Te_6$ has a layered structure with an interlayer distance of 6.8 Å. With TBA^+ cations intercalated, the interlayer spacing of $(TBA)Cr_2Ge_2Te_6$ hybrid superlattice is enlarged to 16.48 Å; (b): Left: The top-view structure of $Cr_2Ge_2Te_6$. The calculated exchange interaction J is indicated; Right: The edge-sharing $CrTe_6$ octahedrons form a honeycomb-like structure in ab-plane and Cr spins interact through indirect 90° super-exchange couplings with Te. (c): The XRD patterns of pristine $Cr_2Ge_2Te_6$ and intercalated $(TBA)Cr_2Ge_2Te_6$ shows a series of (00l) diffractions. The inset shows the images of the single crystal, before and after intercalation. The resulting $(TBA)Cr_2Ge_2Te_6$ samples still maintain a plate-like morphology yet much thicker.

The detailed characterization of $Cr_2Ge_2Te_6$ single crystal are presented in supporting information S2 and S3. The resulting $(TBA)Cr_2Ge_2Te_6$ samples still maintain the well-defined plate-like morphology. The crystal structure of $Cr_2Ge_2Te_6$ is shown in Figure 1a and 1b. Its c-axis parameter is 20.44 Å, corresponding to a unit composed of three $Cr_2Ge_2Te_6$ layers. For the pristine crystal, the distance

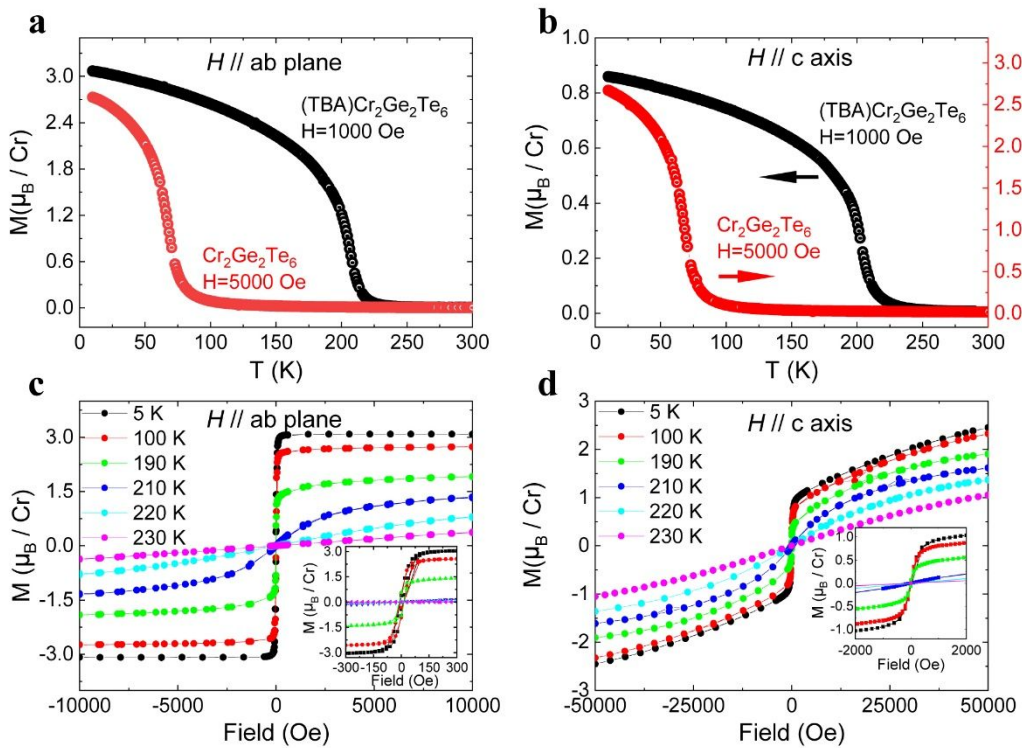


Figure 2. The large increase of Curie temperature and field dependent magnetic susceptibility in (TBA) $\text{Cr}_2\text{Ge}_2\text{Te}_6$. (a) and (b): The temperature dependent magnetic susceptibility (M - T) of pristine $\text{Cr}_2\text{Ge}_2\text{Te}_6$ and (TBA) $\text{Cr}_2\text{Ge}_2\text{Te}_6$ with $H \parallel ab$ and $H \parallel c$, respectively; (c) and (d): The magnetic field dependent magnetic susceptibility (M - H) of (TBA) $\text{Cr}_2\text{Ge}_2\text{Te}_6$ with $H \parallel ab$ and $H \parallel c$, respectively. The insets in c and d show the enlarged views of M - H curves, with $H \parallel ab$ and $H \parallel c$. When $H \parallel ab$, the saturation field and coercive field is 100 Oe and 30 Oe at $T = 5$ K, respectively. For $H \parallel c$, there is nearly no coercive field observed in M - H curves.

between adjacent $\text{Cr}_2\text{Ge}_2\text{Te}_6$ layers is 6.8 Å, as indicated in Figure 1a. After intercalation, as is shown in Figure 1c, the X-ray diffraction (XRD) pattern of (TBA) $\text{Cr}_2\text{Ge}_2\text{Te}_6$ shows (00l) peaks and can be indexed with a c-axis parameter of 49.44 Å (one-unit cell contains three slabs of (TBA) $\text{Cr}_2\text{Ge}_2\text{Te}_6$ and interlayer spacing is 16.48 Å), and the proposed structural model is illustrated in Figure 1a. Given that the size of TBA^+ is around 10 Å (see supporting information S4),²⁰⁻²³ the interlayer spacing of 16.48 Å for the (TBA) $\text{Cr}_2\text{Ge}_2\text{Te}_6$ is the sum of single layer $\text{Cr}_2\text{Ge}_2\text{Te}_6$ and one layer of TBA^+ cations. The interlayer spacing of $\text{Cr}_2\text{Ge}_2\text{Te}_6$ and (TBA) $\text{Cr}_2\text{Ge}_2\text{Te}_6$ was also examined by high resolution transmission electron microscopy (HRTEM) (see supporting information S5). Moreover, from the HRTEM and selected area electron diffraction (SAED) results, the in-plane lattice parameters of (TBA) $\text{Cr}_2\text{Ge}_2\text{Te}_6$ remain almost the same with pristine $\text{Cr}_2\text{Ge}_2\text{Te}_6$. It should be noted that the intercalation of TBA^+ cations would not

lead to the in-plane shift of $\text{Cr}_2\text{Ge}_2\text{Te}_6$, since subsequent low temperature annealing could easily de-intercalate TBA^+ cation and transform (TBA) $\text{Cr}_2\text{Ge}_2\text{Te}_6$ back to pristine $\text{Cr}_2\text{Ge}_2\text{Te}_6$. In fact, in TMD materials such as 2H-TaS₂ or 2H-NbS₂ in which one-unit cell also contains 2 slabs, the organic intercalation does not lead to the in-plane slab shift.^{24,25}

Figure 2 shows temperature-dependent magnetic susceptibility (M - T) for $\text{Cr}_2\text{Ge}_2\text{Te}_6$ and (TBA) $\text{Cr}_2\text{Ge}_2\text{Te}_6$ and field-dependent magnetic susceptibility (M - H) of (TBA) $\text{Cr}_2\text{Ge}_2\text{Te}_6$. In Figure 2a and 2b, the M - T curve of (TBA) $\text{Cr}_2\text{Ge}_2\text{Te}_6$ shows a ferromagnetic order transition with Curie temperature $T_c = 208$ K, which is significantly higher than $T_c = 67$ K in the pristine $\text{Cr}_2\text{Ge}_2\text{Te}_6$.²⁶ Figure 2c exhibits the magnetic field-dependent susceptibility of (TBA) $\text{Cr}_2\text{Ge}_2\text{Te}_6$ at different temperature with $H \parallel ab$ plane.

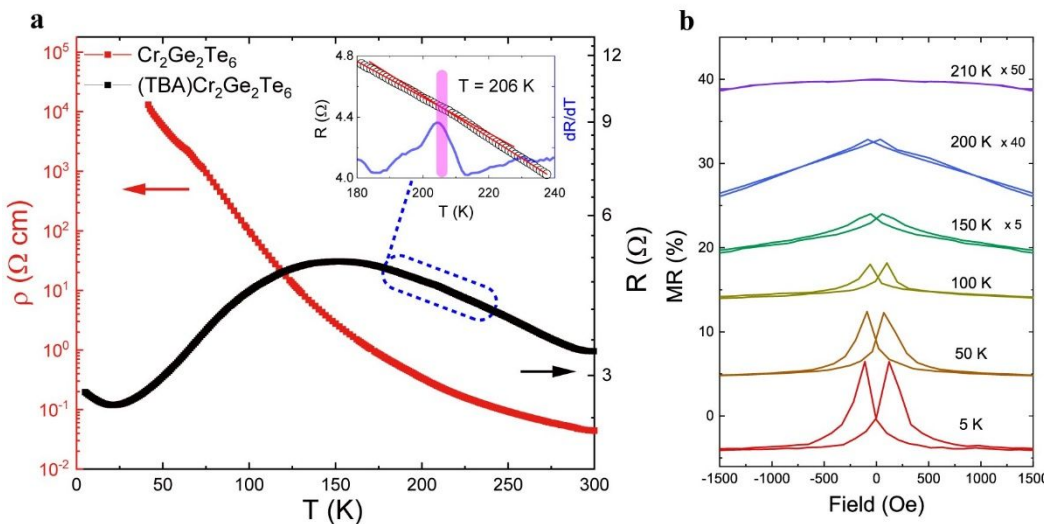


Figure 3. The resistance of $(\text{TBA})\text{Cr}_2\text{Ge}_2\text{Te}_6$. (a): The temperature dependent resistivity of pristine $\text{Cr}_2\text{Ge}_2\text{Te}_6$ and resistance of $(\text{TBA})\text{Cr}_2\text{Ge}_2\text{Te}_6$, respectively. The inset shows the enlarged view of the RT curve for $(\text{TBA})\text{Cr}_2\text{Ge}_2\text{Te}_6$ in the vicinity of the ferromagnetic order temperature. The pink vertical line indicates the ferromagnetic order temperature determined by the peak in differential curve (blue line), which is corresponding to a small kink in RT curve; (b): The magnetic field dependent magnetoresistance (MR) of $(\text{TBA})\text{Cr}_2\text{Ge}_2\text{Te}_6$ at different temperatures. The MR curves are shifted vertically with a step of 10% for clarity. The MR effect disappears above $T = 210 \text{ K}$, suggesting the vanishing of ferromagnetic order.

The inset of Figure 2c shows a typical ferromagnetic behavior with low saturation field of 100 Oe and a small coercive field of 30 Oe at $T = 5 \text{ K}$. The saturation magnetic moment reaches $3.07 \mu_B / \text{Cr}$ at $T = 5 \text{ K}$. In contrast, as shown in supporting information S2, no M - H loop is observed in $\text{Cr}_2\text{Ge}_2\text{Te}_6$ and the saturation field reaches 5000 Oe with $H // ab$ plane at $T = 5 \text{ K}$, which is much larger than that of $(\text{TBA})\text{Cr}_2\text{Ge}_2\text{Te}_6$. The small coercive field in $(\text{TBA})\text{Cr}_2\text{Ge}_2\text{Te}_6$ may originate from the weak pinning of domain walls induced by disorder from organic ion intercalation.²⁷ Compared to the saturation magnetic moment of $2.75 \mu_B/\text{Cr}$ at $T = 5 \text{ K}$ with $H // ab$ -plane in pristine $\text{Cr}_2\text{Ge}_2\text{Te}_6$ (see supporting information S2), the value in $(\text{TBA})\text{Cr}_2\text{Ge}_2\text{Te}_6$ is slightly increased to $3.07 \mu_B/\text{Cr}$ at $T = 5 \text{ K}$ with $H // ab$ plane, indicating the electron doping to $\text{Cr}_2\text{Ge}_2\text{Te}_6$.¹¹ With increasing temperature, the M - H curve is gradually reduced in magnitude and shows linear dependence above $T = 210 \text{ K}$, indicating a ferromagnetic-paramagnetic transition, which is in excellent agreement with M-T curve in Figure 2a. When $H // c$ -axis, the M - H curve shows a different behavior. In Figure 2d, there is no any saturation behavior below 50000 Oe. In contrast, the saturation field is only 100 Oe for $H // ab$ plane, which suggests a large magnetic anisotropy in $(\text{TBA})\text{Cr}_2\text{Ge}_2\text{Te}_6$. Such behavior indicates that the magnetic easy-axis of $(\text{TBA})\text{Cr}_2\text{Ge}_2\text{Te}_6$ lies in the ab plane, whereas the easy-axis of $\text{Cr}_2\text{Ge}_2\text{Te}_6$ is along c -axis.²⁶ Moreover, the M - H curve with $H // c$ axis resembles the

features in $\text{Cr}_{1/3}\text{TaS}_2$, in which a steeper slope could be observed in the low-field region.²⁸ This feature could be due to the existence of misoriented domains in samples.²⁸ In addition, by fitting the temperature-dependent inverse susceptibility with Curie-Weiss law (see supporting information S6), we obtained effective magnetic moment $\mu_{\text{eff}} \sim 4.20 \mu_B / \text{Cr}$ with $H // ab$ -plane and $4.18 \mu_B / \text{Cr}$ with $H // c$ -axis.

Since the Curie temperature is largely increased from 67 K in $\text{Cr}_2\text{Ge}_2\text{Te}_6$ to 208 K in intercalated $(\text{TBA})\text{Cr}_2\text{Ge}_2\text{Te}_6$, one major concern would be whether the high- T_c is originated from $(\text{TBA})\text{Cr}_2\text{Ge}_2\text{Te}_6$ or impurity phases. It is reported that Fe_3GeTe_2 would decompose upon Na-intercalation.²⁹ Moreover, numerous CrTe_x phases also exhibits high T_c .^{30,31} In order to rule out the possibility of impurity phase or obvious deficiency, detailed chemical and structure characterizations were conducted. The combination of CHN analysis, Energy Dispersive Spectroscopy (EDS) and thermo-gravimetric analysis (TGA) (see supporting information S5 and S7) gives the composition of intercalated compounds to be $(\text{TBA})\text{Cr}_2\text{Ge}_2\text{Te}_6$, being consistent with our assumption. Moreover, HRTEM and EDS confirms that there is no obvious impurity phase or deficiency in intercalated compounds. Most importantly, by annealing the $(\text{TBA})\text{Cr}_2\text{Ge}_2\text{Te}_6$ at 150 °C, the magnetic properties as well as structure of $(\text{TBA})\text{Cr}_2\text{Ge}_2\text{Te}_6$ could fully reverse back to pristine $\text{Cr}_2\text{Ge}_2\text{Te}_6$, with TBA⁺ cations

de-intercalated (see supporting information S8). The annealing experiment

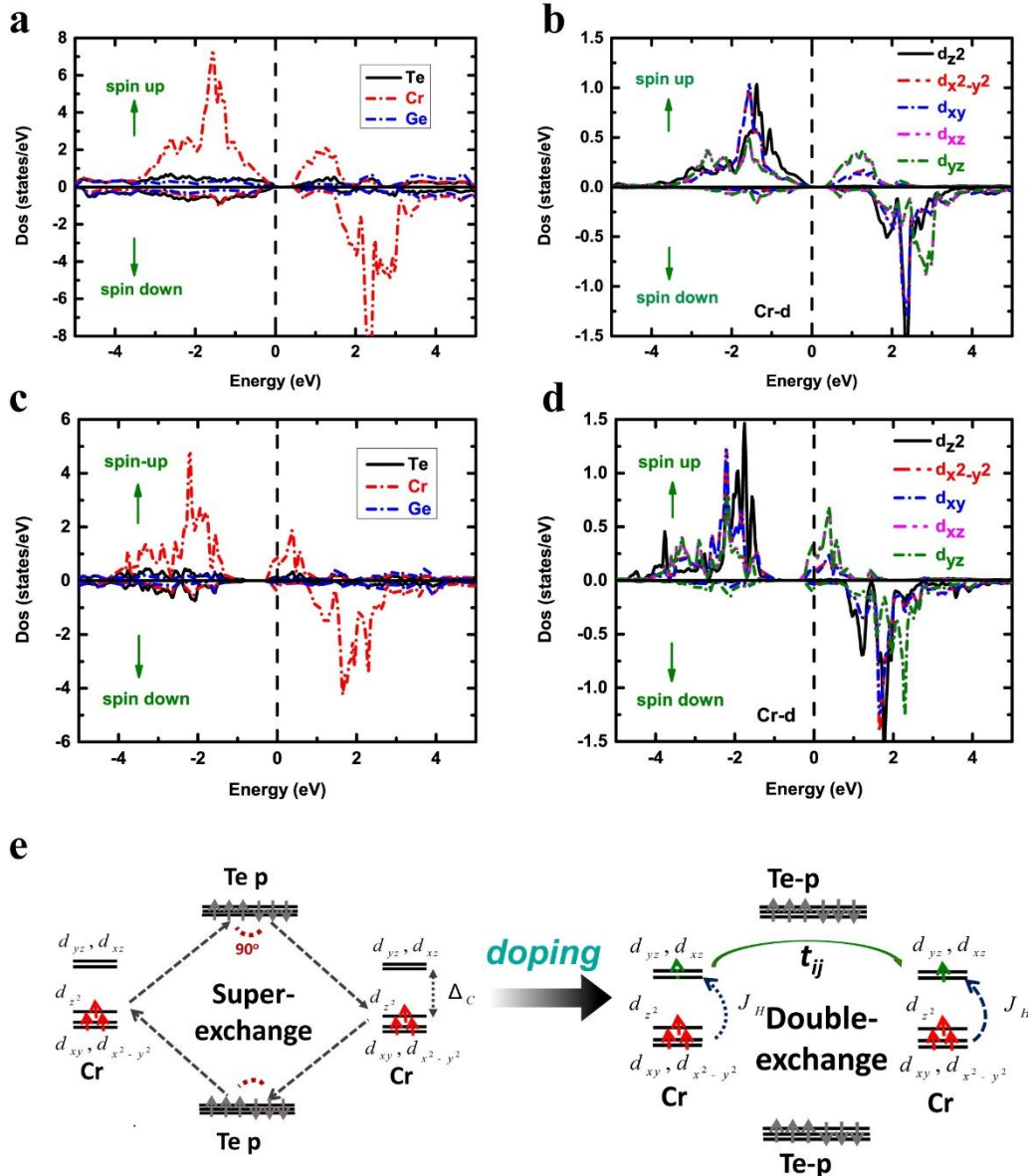


Figure 4. Electronic structures of $\text{Cr}_2\text{Ge}_2\text{Te}_6$ and $(\text{TBA})\text{Cr}_2\text{Ge}_2\text{Te}_6$. (a): Element-resolved polarized density of states (PDOS) of pristine $\text{Cr}_2\text{Ge}_2\text{Te}_6$; (b): Cr's orbital-resolved PDOS of $\text{Cr}_2\text{Ge}_2\text{Te}_6$; (c): Element-resolved PDOS of $(\text{TBA})\text{Cr}_2\text{Ge}_2\text{Te}_6$; (d): Cr's orbital-resolved PDOS of $(\text{TBA})\text{Cr}_2\text{Ge}_2\text{Te}_6$; (e): Schematic diagrams of the super-exchange interaction in $\text{Cr}_2\text{Ge}_2\text{Te}_6$ and the double-exchange interaction in $(\text{TBA})\text{Cr}_2\text{Ge}_2\text{Te}_6$. t_{ij} represents the hopping amplitude and J_H is Hund coupling. For (a)-(d), the up/down arrows indicates the majority and minority spins.

ambiguously proves that the observed ferromagnetic order at 208 K is originated from the intercalation of TBA⁺ cations in $(\text{TBA})\text{Cr}_2\text{Ge}_2\text{Te}_6$.

Figure 3a shows temperature-dependent resistance of $(\text{TBA})\text{Cr}_2\text{Ge}_2\text{Te}_6$ and $\text{Cr}_2\text{Ge}_2\text{Te}_6$. $\text{Cr}_2\text{Ge}_2\text{Te}_6$ shows a typical semiconducting behavior with a small kink at 65 K, corresponding to the ferromagnetic order temperature. By fitting the data with thermal activation model, we

obtained an energy gap of 0.2 eV for $\text{Cr}_2\text{Ge}_2\text{Te}_6$, which is in excellent agreement with previous reports (see supporting information S3).^{15,26} The resistance of $(\text{TBA})\text{Cr}_2\text{Ge}_2\text{Te}_6$ shows a metallic behavior with a broad hump around 150 K, in sharp contrast to the semiconducting behavior in $\text{Cr}_2\text{Ge}_2\text{Te}_6$. Around $T = 206$ K, we observe one kink in R-T curve and its first derivative curve (see the inset of Figure 3a), indicating the Curie temperature. Besides, there is a little upturn of resistance

at low temperatures for $(TBA)Cr_2Ge_2Te_6$. This feature is similar to that observed in Fe_3GeTe_2 grown by molecular beam epitaxy and could be due to disorder effect.³² Heat capacity measurements were also carried out to confirm the ferromagnetic order in $(TBA)Cr_2Ge_2Te_6$, which is shown in supporting information S9.

Magnetic field dependent transverse magnetoresistance (MR) were measured to verify the ferromagnetic order in $(TBA)Cr_2Ge_2Te_6$. As shown in Figure 3b, a clear butterfly-shaped hysteresis shows up at low temperatures, which is due to spin-dependent scattering of carriers by local magnetic ordering.³³ These data confirm the existence of long-range ferromagnetic order. The peak in MR corresponds to the coercive field (H_c), and it is gradually reduced with increasing temperature and eventually vanishes above $T = 210$ K. These results are highly consistent with the behavior of magnetic susceptibility.

In order to reveal the mechanism of the large enhancement of T_c as well as the orientation of the easy axis in $(TBA)Cr_2Ge_2Te_6$, first-principles calculations were performed to investigate the electronic and magnetic structures of $(TBA)Cr_2Ge_2Te_6$. The structure of $(TBA)Cr_2Ge_2Te_6$ is modeled using the slab superlattice approach with the experimental determined interlayer space. Charge doping induced by the intercalation was taken into account using the charged cell method. The details of the model could be found in supporting information S10. The magnetic anisotropy energy (MAE) was calculated through the total energy difference for two magnetization directions, $\langle 001 \rangle$ (perpendicular to the quasi-2D plane) and $\langle 100 \rangle$ (arbitrarily chosen in the plane). The energy of MAE, $\Delta E = E_{001} - E_{100}$, of pristine $Cr_2Ge_2Te_6$ equals to -0.063 meV/Cr, indicating that the magnetization orientation prefers the c-axis. In contrast, the MAE of $(TBA)Cr_2Ge_2Te_6$ is $\Delta E = 0.591$ meV/Cr, suggesting that the magnetization prefers to point in the ab-plane. These results are consistent with the experimental finding.

To estimate the magnetic ordering temperature (T_c) of both pristine and intercalated $Cr_2Ge_2Te_6$, based on the magnetic energy of the *ab initio* calculations, we calculated the nearest Cr's exchange coupling parameter by mapping the calculated total energies of ferromagnetic and antiferromagnetic configurations onto the classical Heisenberg Hamiltonian $H = \sum_{\langle i,j \rangle} J S_i \cdot S_j$, in which S_i is the spin operator on site i. The ferromagnetic coupling strengths are $-J_0 = 10.21$ meV and $-J_{intercal} = 19.69$ meV before and after intercalation, respectively. This finding suggests that the ferromagnetic Curie temperature T_c increases strikingly when $Cr_2Ge_2Te_6$ is intercalated with TBA⁺ cation.

To account for the experimental observations on the magnetic easy-axis switching and the considerable increase of the T_c , we calculated the polarized density of states (PDOS) and Cr's orbital-resolved PDOS for $Cr_2Ge_2Te_6$ and $(TBA)Cr_2Ge_2Te_6$, as shown in Figure 4(a-d). Moreover, band structure and spin-polarized full DOS of $Cr_2Ge_2Te_6$ and $(TBA)Cr_2Ge_2Te_6$ are shown in supporting information S11 and S12. We find that after intercalation, $Cr_2Ge_2Te_6$ slab is electron-doped, with the ground state of the compound altering from insulator to metal, as shown in Figure 4(c). This could also be supported by Raman spectroscopy and X-ray photoelectron spectroscopy (XPS) (See supporting information S13). Moreover, the major DOS contribution near Fermi-level originates from previous unoccupied Cr d_{xz} and d_{yz} orbits. These conducting Cr d_{xz} and d_{yz} would generate the Hund's coupling exchanges with other local spins of Cr, which is illustrated in Figure 4(e). This scenario is just in accordance with double-exchange ferromagnetism interaction mechanism proposed by Anderson and Hasegawa.³⁴ Therefore, the magnetic coupling strength between Cr spins significantly increases due to direct coupling, which gives rise to the huge enhancement of Curie temperature.

Regarding the magnetic easy-axis switching, before intercalation, the Cr spins mainly interact via the indirect Cr-Te-Cr through indirect 90° super-exchange couplings, e.g., $Cr d_z^2$ -ligand Te p-Cr d_z^2 , which leads to the weak FM coupling and c-axis anisotropy by the ligand p spin-orbit coupling. After intercalation, the major DOS contribution comes from the conducting d_{xz} and d_{yz} orbital components, as shown in Figure 4d. Based on our calculation result, the doublet d_{xz}/d_{yz} orbitals combining other 3d orbital components would contribute an effective non-zero orbital moment with $L/c = 0.0058 \mu_B$ and $L/a = 0.0281 \mu_B$, mainly lying on the ab-plane. Taking into account the spin-orbit coupling of Cr ions, the planar orbital moment component pushes the spin aligned from the c-axis to the ab-plane. Hence, it is the spin-orbit coupling (SOC) of Cr ions as well as the double-exchange interaction that switch the easy axis orientation from the c-axis to ab-plane, leading to the magnetic easy-axis switching to the ab-plane.

In previous studies, the modulation of magnetic properties for $Cr_2Ge_2Te_6$ has been attempted by traditional metal-insulator semiconductor (MIS) FET and hydrostatic pressure.^{11,35} For MIS-FET, the tuning effect is relatively weak due to the limited charge doping.¹¹ By applying hydrostatic pressure, the insulating behavior of $Cr_2Ge_2Te_6$ is gradually suppressed, and the easy-axis orientation changes from c-axis to ab-plane due to the increase of off-site spin-orbit interaction of Te atoms with the compressed Cr-Te distance.³⁵ However, T_c is nearly

unchanged under pressure. In our studies, the Curie temperature of $\text{Cr}_2\text{Ge}_2\text{Te}_6$ shows a huge increase upon the organic ion intercalation. To our best knowledge, this approach has not been reported in other van der Waals magnetic crystals. Our studies indicate that electrochemical intercalation of organic ions is an effective and convenient way in tuning the magnetic properties of layered materials.

CONCLUSIONS

In summary, we successfully intercalated organic ion tetrabutyl ammonium (TBA^+) into the van der Waals gap of $\text{Cr}_2\text{Ge}_2\text{Te}_6$ and form the hybrid superlattice $(\text{TBA})\text{Cr}_2\text{Ge}_2\text{Te}_6$. Surprisingly, $(\text{TBA})\text{Cr}_2\text{Ge}_2\text{Te}_6$ shows a metallic behavior at low temperatures and the Curie temperature is significantly increased from 67 K in pristine $\text{Cr}_2\text{Ge}_2\text{Te}_6$ to 208 K. The magnetic easy axis of $(\text{TBA})\text{Cr}_2\text{Ge}_2\text{Te}_6$ is reoriented to ab plane in contrast to the c-axis in pristine $\text{Cr}_2\text{Ge}_2\text{Te}_6$. Transport measurement and theoretical calculations indicate that the electron doping in $\text{Cr}_2\text{Ge}_2\text{Te}_6$ leads to the transition from insulator to metal, and consequently the underlying mechanism of the ferromagnetism is changed from weak super-exchange mediated ferromagnetism in $\text{Cr}_2\text{Ge}_2\text{Te}_6$ to the metallic double-exchange ferromagnetism in $(\text{TBA})\text{Cr}_2\text{Ge}_2\text{Te}_6$. This change leads to a drastic increase of Curie temperature upon intercalation of TBA^+ . Our studies suggest that the magnetic properties of magnetic van der Waals materials could be remarkably tuned by the electrochemical intercalation of organic molecules, which paves a new way to manipulate the magnetic and electronic properties in magnetic van der Waals crystals.

ASSOCIATED CONTENT

Supporting Information.

The Supporting Information is available free of charge on the ACS Publications website at DOI: XXXXX.

Discharge curve of $(\text{TBA})\text{Cr}_2\text{Ge}_2\text{Te}_6$; Characterization of $\text{Cr}_2\text{Ge}_2\text{Te}_6$; Structure of TBA^+ ; HRTEM images; Curie-Weiss fitting of $(\text{TBA})\text{Cr}_2\text{Ge}_2\text{Te}_6$; TGA analysis; Annealing experiment of $(\text{TBA})\text{Cr}_2\text{Ge}_2\text{Te}_6$; Heat capacity of $\text{Cr}_2\text{Ge}_2\text{Te}_6$ and $(\text{TBA})\text{Cr}_2\text{Ge}_2\text{Te}_6$; Theoretical calculation details; Band structure, pDOS of $\text{Cr}_2\text{Ge}_2\text{Te}_6$ and $(\text{TBA})\text{Cr}_2\text{Ge}_2\text{Te}_6$; Raman spectroscopy, XPS, and FT-IR of $\text{Cr}_2\text{Ge}_2\text{Te}_6$ and $(\text{TBA})\text{Cr}_2\text{Ge}_2\text{Te}_6$.

AUTHOR INFORMATION

Corresponding Author

* zou@theory.issp.ac.cn

* chenxh@ustc.edu.cn

Author Contributions

†These authors contribute equally to this work.

Notes

The authors declare no competing financial interest.

ACKNOWLEDGMENT

We would also like to thank Binghui Ge, Haifeng Du and Shasha Wang for their help on TEM experiments. This work is supported by the National Key R&D Program of China (Grant Nos. 2016YFA0300201, 2017YFA0303001 and 2017YFA0403503), the National Natural Science Foundation of China (Grant Nos. 11534010 and 11888101), the Key Research Program of Frontier Sciences, CAS, China (QYZDY-SSW-SLH021), the Strategic Priority Research Program (B) of the Chinese Academy of Sciences (Grant No. XDB25010100), Science Challenge Project (Grants No. TZ2016004), and Hefei Science Center CAS (2016HSC-IU001).

REFERENCES

- (1)Novoselov, K. S.; Geim, A. K.; Morozov, S. V.; Jiang, D.; Zhang, Y.; Dubonos, S. V.; Grigorieva, I. V.; Firsov, A. A., Electric field effect in atomically thin carbon films. *Science* **2004**, 306 (5696), 666-9.
- (2)Li, L. K.; Yu, Y. J.; Ye, G. J.; Ge, Q. Q.; Ou, X. D.; Wu, H.; Feng, D. L.; Chen, X. H.; Zhang, Y. B., Black phosphorus field-effect transistors. *Nat Nanotechnol* **2014**, 9 (5), 372-377.
- (3)Duong, D. L.; Yun, S. J.; Lee, Y. H., van der Waals Layered Materials: Opportunities and Challenges. *Acs Nano* **2017**, 11 (12), 11803-11830.
- (4)Burch, K. S.; Mandrus, D.; Park, J. G., Magnetism in two-dimensional van der Waals materials. *Nature* **2018**, 563 (7729), 47-52.
- (5)Gong, C.; Li, L.; Li, Z.; Ji, H.; Stern, A.; Xia, Y.; Cao, T.; Bao, W.; Wang, C.; Wang, Y.; Qiu, Z. Q.; Cava, R. J.; Louie, S. G.; Xia, J.; Zhang, X., Discovery of intrinsic ferromagnetism in two-dimensional van der Waals crystals. *Nature* **2017**, 546 (7657), 265-269.
- (6)Huang, B.; Clark, G.; Navarro-Moratalla, E.; Klein, D. R.; Cheng, R.; Seyler, K. L.; Zhong, D.; Schmidgall, E.; McGuire, M. A.; Cobden, D. H.; Yao, W.; Xiao, D.; Jarillo-Herrero, P.; Xu, X., Layer-dependent ferromagnetism in a van der Waals crystal down to the monolayer limit. *Nature* **2017**, 546 (7657), 270-273.
- (7)Deng, Y.; Yu, Y.; Song, Y.; Zhang, J.; Wang, N. Z.; Sun, Z.; Yi, Y.; Wu, Y. Z.; Wu, S.; Zhu, J.; Wang, J.; Chen, X. H.; Zhang, Y., Gate-tunable room-temperature ferromagnetism in two-dimensional Fe_3GeTe_2 . *Nature* **2018**, 563 (7729), 94-99.
- (8)Huang, B.; Clark, G.; Klein, D. R.; MacNeill, D.; Navarro-Moratalla, E.; Seyler, K. L.; Wilson, N.; McGuire, M. A.; Cobden, D. H.; Xiao, D.; Yao, W.; Jarillo-Herrero, P.; Xu, X., Electrical control of 2D magnetism in bilayer CrI_3 . *Nat Nanotechnol* **2018**, 13 (7), 544-548.
- (9)Jiang, S.; Li, L.; Wang, Z.; Mak, K. F.; Shan, J., Controlling magnetism in 2D CrI_3 by electrostatic doping. *Nat Nanotechnol* **2018**, 13 (7), 549-553.

- (10) Jiang, S.; Shan, J.; Mak, K. F., Electric-field switching of two-dimensional van der Waals magnets. *Nat Mater* **2018**, *17* (5), 406-410.
- (11) Wang, Z.; Zhang, T.; Ding, M.; Dong, B.; Li, Y.; Chen, M.; Li, X.; Huang, J.; Wang, H.; Zhao, X.; Li, Y.; Li, D.; Jia, C.; Sun, L.; Guo, H.; Ye, Y.; Sun, D.; Chen, Y.; Yang, T.; Zhang, J.; Ono, S.; Han, Z.; Zhang, Z., Electric-field control of magnetism in a few-layered van der Waals ferromagnetic semiconductor. *Nat Nanotechnol* **2018**, *13* (7), 554-559.
- (12) Wan, C.; Gu, X.; Fang, F.; Itoh, T.; Wang, Y.; Sasaki, H.; Kondo, M.; Koga, K.; Yabuki, K.; Snyder, G. J.; Yang, R.; Koumoto, K., Flexible n-type thermoelectric materials by organic intercalation of layered transition metal dichalcogenide TiS₂. *Nat Mater* **2015**, *14* (6), 622-7.
- (13) Shi, M. Z.; Wang, N. Z.; Lei, B.; Shang, C.; Meng, F. B.; Ma, L. K.; Zhang, F. X.; Kuang, D. Z.; Chen, X. H., Organic-ion-intercalated FeSe-based superconductors. *Phys Rev Mater* **2018**, *2* (7), 074801.
- (14) Wang, N. Z.; Shi, M. Z.; Shang, C.; Meng, F. B.; Ma, L. K.; Luo, X. G.; Chen, X. H., Tunable superconductivity by electrochemical intercalation in TaS₂. *New J Phys* **2018**, *20*, 023014.
- (15) Ji, H. W.; Stokes, R. A.; Alegria, L. D.; Blomberg, E. C.; Tanatar, M. A.; Reijnders, A.; Schoop, L. M.; Liang, T.; Prozorov, R.; Burch, K. S.; Ong, N. P.; Petta, J. R.; Cava, R. J., A ferromagnetic insulating substrate for the epitaxial growth of topological insulators. *J Appl Phys* **2013**, *114* (11), 114707.
- (16) Zhu, G.; Liu, J.; Zheng, Q.; Zhang, R.; Li, D.; Banerjee, D.; Cahill, D. G., Tuning thermal conductivity in molybdenum disulfide by electrochemical intercalation. *Nat Commun* **2016**, *7*, 13211.
- (17) Hitz, E.; Wan, J.; Patel, A.; Xu, Y.; Meshi, L.; Dai, J.; Chen, Y.; Lu, A.; Davydov, A. V.; Hu, L., Electrochemical Intercalation of Lithium Ions into NbSe₂ Nanosheets. *ACS Appl Mater Interfaces* **2016**, *8* (18), 11390-5.
- (18) Blaha, P., An augmented plane wave+ local orbitals program for calculating crystal properties, Karlheinz Schwarz, Techn. Universität Wien, Austria **2001**.
- (19) Perdew, J. P.; Burke, K.; Ernzerhof, M., Generalized Gradient Approximation Made Simple. *Phys Rev Lett* **1996**, *77* (18), 3865-3868.
- (20) Gao, Q. M.; Giraldo, O.; Tong, W.; Suib, S. L., Preparation of nanometer-sized manganese oxides by intercalation of organic ammonium ions in synthetic birnessite OL-1. *Chem Mater* **2001**, *13* (3), 778-786.
- (21) Omomo, Y.; Sasaki, T.; Wang, L.; Watanabe, M., Redoxable nanosheet crystallites of MnO₂ derived via delamination of a layered manganese oxide. *J Am Chem Soc* **2003**, *125* (12), 3568-75.
- (22) Kim, H. N.; Keller, S. W.; Mallouk, T. E.; Schmitt, J.; Decher, G., Characterization of zirconium phosphate polycation thin films grown by sequential adsorption reactions. *Chem Mater* **1997**, *9* (6), 1414-1421.
- (23) Sugimoto, W.; Iwata, H.; Yasunaga, Y.; Murakami, Y.; Takasu, Y., Preparation of ruthenic acid nanosheets and utilization of its interlayer surface for electrochemical energy storage. *Angew Chem Int Ed* **2003**, *42* (34), 4092-6.
- (24) Gamble, F. R.; Osiecki, J. H.; Disalvo, F. J., Some Superconducting Intercalation Complexes of TaS₂ and Substituted Pyridines. *J Chem Phys* **1971**, *55* (7), 3525-&.
- (25) Boller, H.; Blaha, H., Intercalation Phases of TiS₂, 2H-NbS₂, and 1T-TaS₂ with Ethylenediamine and Trimethylenediamine - a Crystal Chemical and Thermogravimetric Study. *J Solid State Chem* **1982**, *45* (1), 119-126.
- (26) Lin, G. T.; Zhuang, H. L.; Luo, X.; Liu, B. J.; Chen, F. C.; Yan, J.; Sun, Y.; Zhou, J.; Lu, W. J.; Tong, P.; Sheng, Z. G.; Qu, Z.; Song, W. H.; Zhu, X. B.; Sun, Y. P., Tricritical behavior of the two-dimensional intrinsically ferromagnetic semiconductor CrGeTe₃. *Phys Rev B* **2017**, *95* (24), 245212.
- (27) Kittel, C., Physical Theory of Ferromagnetic Domains. *Rev Mod Phys* **1949**, *21* (4), 541-583.
- (28) Yamasaki, Y.; Moriya, R.; Arai, M.; Masubuchi, S.; Pyon, S.; Tamegai, T.; Ueno, K.; Machida, T., Exfoliation and van der Waals heterostructure assembly of intercalated ferromagnet Cr_{1/3}TaS₂. *2d Mater* **2017**, *4* (4), 041007.
- (29) Weber, D.; Trout, A. H.; McComb, D. W.; Goldberger, J. E., Decomposition-Induced Room-Temperature Magnetism of the Na-Intercalated Layered Ferromagnet Fe_{3-x}GeTe₂. *Nano Lett* **2019**, *19* (8), 5031-5035.
- (30) Lukoschus, K.; Kraschinski, S.; Nather, C.; Bensch, W.; Kremer, R. K., Magnetic properties and low temperature X-ray studies of the weak ferromagnetic monoclinic and trigonal chromium tellurides Cr₅Te₈. *J Solid State Chem* **2004**, *177* (3), 951-959.
- (31) Liu, Y.; Petrovic, C., Critical behavior of the quasi-two-dimensional weak itinerant ferromagnet trigonal chromium telluride Cr_{0.62}Te. *Phys Rev B* **2017**, *96* (13), 134410.
- (32) Liu, S.; Yuan, X.; Zou, Y.; Sheng, Y.; Huang, C.; Zhang, E.; Ling, J.; Liu, Y.; Wang, W.; Zhang, C.; Zou, J.; Wang, K.; Xiu, F., Wafer-scale two-dimensional ferromagnetic Fe₃GeTe₂ thin films grown by molecular beam epitaxy. *npj 2D Materials and Applications* **2017**, *1* (1), 30.
- (33) Zhang, Z. C.; Feng, X.; Guo, M. H.; Li, K.; Zhang, J. S.; Ou, Y. B.; Feng, Y.; Wang, L. L.; Chen, X.; He, K.; Ma, X. C.; Xue, Q. K.; Wang, Y. Y., Electrically tuned magnetic order and magnetoresistance in a topological insulator. *Nat Commun* **2014**, *5*, 4915.
- (34) Anderson, P. W.; Hasegawa, H., Considerations on Double Exchange. *Phys Rev* **1955**, *100* (2), 675-681.
- (35) Lin, Z. S.; Lohmann, M.; Ali, Z. A.; Tang, C.; Li, J. X.; Xing, W. Y.; Zhong, J. N.; Jia, S.; Han, W.; Coh, S.; Beyermann, W.; Shi, J., Pressure-induced spin reorientation transition in layered ferromagnetic insulator Cr₂Ge₂Te₆. *Phys Rev Mater* **2018**, *2* (5).

1 “For Table of Contents Only”
2
3
4
5
6
7
8
9
10
11
12
13
14

